

Characterization of Sm-Doped Ceria Ceramics Synthesized by Two Different Methods

Aliye Arabaci and Özgün Serin

(Submitted March 13, 2015; in revised form April 29, 2015; published online June 5, 2015)

Ceria-based materials have attracted much attention as electrolyte materials for low and intermediate temperature solid oxide fuel cells (SOFCs). In this study, we examined the effect of synthesis method on the microstructure and the ionic conductivity of ceria-based electrolytes. $\text{Sm}_{0.2}\text{Ce}_{0.8}\text{O}_{1.9}$ (SDC) electrolytes for SOFCs were prepared using the Pechini and cellulose templating (CT) methods. Microstructures of the calcined and sintered samples were characterized by XRD and SEM techniques. The XRD results indicate that a single-phase fluorite structure formed at the relatively low calcination temperature of 500 °C. The relative densities of the sintered pellets were higher than 90%, which was proved by the SEM images. Calcined powders were characterized by FTIR technique. The electrical properties of the samarium-doped ceria electrolytes were analyzed by electrochemical impedance spectroscopy. The total ionic conductivities are 3.02×10^{-2} and 3.42×10^{-2} S/cm at 750 °C for the SDC electrolytes prepared by the Pechini method and the CT method, respectively.

Keywords cellulose templating method, electrolyte materials, Pechini method, samarium-doped ceria

1. Introduction

Solid oxide fuel cells (SOFCs) have attracted much attention as a promising source of electrical power generation due to their high efficiency in converting chemical energy into electrical energy by electrochemical reactions. In general, conventional SOFCs that use yttria-stabilized zirconia (YSZ) as an electrolyte material operate at approximately 1000 °C (Ref 1, 2). However, operation at such high temperatures causes material degradation, as well as other technological complications and economic obstacles. Therefore, the development of new electrolyte materials for SOFCs that operate at lower temperatures is needed. In this context, ceria-based materials have great potential as electrolytes for SOFCs that operate at lower temperatures (Ref 3-6). The ionic conductivity of ceria increases significantly with the oxygen vacancies created by the doping of rare earth cations into the ceria lattice. The ionic conductivity at 750 °C of doped ceria is similar to that of yttria-stabilized zirconia at 1000 °C (Ref 7). Among the various dopants used, Sm^{3+} , Dy^{3+} , and Gd^{3+} are favorable for increasing the ionic conductivity (Ref 8, 9).

To synthesize ceria-based electrolytes with the desired properties, various methods such as urea combustion, citrate-nitrate combustion, precipitation, microwave-induced combustion, hydrothermal synthesis, flame-spray pyrolysis, sol-gel, ultrasound-microwave assisted sol-gel, and carbonate precipitation (Ref 10-18) have been employed. Phase purity, stability, and relative density are the important factors for obtaining high

performance doped ceria electrolytes. The aforesaid techniques require much time and high amounts of energy for the calcination and sintering process. Compared to other preparation methods, the well-known Pechini and cellulose templating (CT) methods have numerous advantages. A fast and facile CT method allows the formation of mixed oxide structures (Ref 19), which could be used as SOFC components, with high phase purity, even at relatively low calcination temperatures. This method consists of three steps: soaking of stoichiometric solution into a cellulose paper, drying, and combustion/calcination. Compared with many chemical routes, the Pechini method is a simple, feasible, and less time consuming technique for preparing various oxide ceramics with direct and precise control over stoichiometry, homogeneity, and purity.

In this work, two different methods (CT method and Pechini method) were used to synthesize samarium-doped ceria solid electrolyte materials. The effect of the synthesis technique on the microstructure and electrical properties of the samarium-doped ceria was investigated. The synthesized powders were calcined at 500 °C for 4 h and then pressed and sintered at 1400 °C for 6 h.

2. Experimental

2.1 Sample Preparation

$\text{Sm}_{0.2}\text{Ce}_{0.8}\text{O}_{1.9}$ solid electrolytes were synthesized using two different synthesis techniques.

2.1.1 SDC Synthesis via Cellulose Templating Method. $\text{Sm}_{0.2}\text{Ce}_{0.8}\text{O}_{1.9}$ solid electrolyte was synthesized with the fast and facile CT method. The CT method is a simple technique to synthesize oxide-structured materials. In this method, stoichiometric amounts of $\text{Ce}(\text{NO}_3)_3 \cdot 6\text{H}_2\text{O}$ (Sigma-Aldrich, 99.999%) and $\text{Sm}(\text{NO}_3)_3 \cdot 6\text{H}_2\text{O}$ (Sigma-Aldrich, 99.999%) salts were dissolved in de-ionized water to produce a 0.35 M (Ref 20) mixed salt stock solution. The solution was soaked into round ashless cellulose filter paper with 125 mm diameter and 0.2 mm thickness (pore size $\leq 2 \mu\text{m}$, Macherey-Nagel,

Aliye Arabaci and Özgün Serin, Department of Metallurgical Engineering, Faculty of Engineering, Istanbul University, Avcilar, 34320 Istanbul, Turkey. Contact e-mail: aliye@istanbul.edu.tr

MN 640 de) at a concentration of 1 mL solution per filter paper. The solution-impregnated papers were then put into a pre-heated furnace and calcined for 4 h at 500 °C. This directly calcined Sm_{0.2}Ce_{0.8}O_{1.9} powder was ground in an agate mortar.

2.1.2 SDC Synthesis via Pechini Method. The material was also prepared using the Pechini method. In this synthesis method, the cerium and samarium nitrate salts were weighed and dissolved into de-ionized water individually at the desired concentrations, and then the solutions were mixed in a beaker. Anhydrous citric acid (Boehringer Ingelheim) was dissolved in de-ionized water and was then added with ethylene glycol (R.P. Normopur) to the cation solution. The molar ratios of total oxide (TO):citric acid (CA) and ethylene glycol:citric acid were 2:1 and 4:1, respectively. The solutions were heated and stirred on a hot plate at 85 °C for 3 h. With the evaporation of water, the solution was gradually transformed into a viscous yellow gel. The gel was placed in an oven and heated at 110 °C for 24 h. Afterwards, the conversion of the so-prepared amorphous precursors into crystalline samarium-doped ceria was achieved by heating the dried solids at a heating rate of 5 °C min⁻¹ to 500 °C and keeping them at this calcination temperature for 4 h.

After that, the calcined powders obtained by both synthesis methods were isostatically cold-pressed under 200 MPa (after first being pressed with a pellet die to produce a pellet shape under 2 MPa). All obtained pellets were sintered at 1400 °C for 6 h. The synthesized powders were labeled according to the synthesis techniques, SDC-PM (Sm_{0.2}Ce_{0.8}O_{1.9} (SDC) synthesized by the Pechini method (PM)) and SDC-CTM (Sm_{0.2}Ce_{0.8}O_{1.9} (SDC) synthesized by the CT method (CTM)).

2.2 Characterization of the Samples

XRD was used to determine the crystal structure of the crystalline phases. X-ray spectra of samarium-doped ceria powders were obtained over the 2θ range of 10°-90° by using a Rigaku D/Max-2200 PC x-ray diffractometer with Cu Kα radiation. The average crystallite diameter of the calcined samples was calculated by using the Scherrer method, $d = K\lambda/\beta\cos\theta$, where K is a constant taken to be 0.9, d is the crystallite size (nm), λ is the wavelength of the radiation (1.5418 Å), β is the corrected peak at full width at half maximum (FWHM) intensity, and θ is the scattering angle of the main reflection (111).

The lattice parameters of the sintered samples were calculated from the peak positions in the diffraction patterns according to Eq (1) (Ref 21, 22):

$$a = d\sqrt{h^2 + k^2 + l^2}, \quad (\text{Eq 1})$$

where a is the cubic lattice parameter; d is the spacing between the planes in the atomic lattice, which is calculated by Bragg's law (Eq 2), and h , k , and l are the Miller indices of the plane.

$$d = \lambda/2 \sin \theta, \quad (\text{Eq 2})$$

where d is the planar spacing, λ is the wavelength of the radiation, θ is the diffraction angle, and a is the lattice parameter.

The densities of the sintered pellets were measured by the Archimedes method. The density measurement was repeated five times for each sample, and the average values were taken. The theoretical density of the samples was calculated using

Eq (3). The densification of samples was determined by dividing the measured density by the theoretical density. The theoretical densities of the samples were taken as 7.15 and 7.20 g cm⁻³ for SDC-CTM and SDC-PM, respectively. These values were calculated by using the lattice parameters determined using the XRD data of the sintered samples, $a = 5.432$ Å for SDC-CTM and $a = 5.418$ Å for SDC-PM

$$D = \frac{4xM_{\text{Sm}} + 4(1-x)M_{\text{Ce}} + 4(2-x/2)M_{\text{O}}}{N_{\text{A}}(a^3)}. \quad (\text{Eq 3})$$

The structural features of the SDC-PM and SDC-CTM powders calcined at 500 °C were characterized by Perkin-Elmer FTIR (Spectrum 100) spectroscopy using the KBr pellet method in the range of 400-4000 cm⁻¹.

The microstructural features of the calcined and sintered SDC-PM and SDC-CTM samples were investigated by scanning electron microscopy (SEM). The SEM analysis was performed with an FEI-QUANTA FEG 450 by examining the outer surface of the pellets. All of the samples were coated with ultra-thin gold films to prevent the accumulation of electrostatic charge on the surface.

Electrochemical impedance spectroscopy (EIS) was used to study the conductivity of the SDC-PM and SDC-CTM pellets in the temperature range of 250-750 °C in air using an AC impedance analyzer (Solartron 1260 FRA and 1296 Interface). To measure the ionic conductivity of the sintered pellets, silver paste was applied to both sides of the pellets as electrodes by firing at 800 °C for half an hour.

3. Results and Discussion

3.1 Powder Characterization

The XRD patterns of the calcined and sintered SDC-CTM and SDC-PM samples are provided in Fig. 1(a) and (b). Calcined SDC-PM and SDC-CTM powders and sintered SDC-PM and SDC-CTM pellets crystallized in the cubic fluorite structure (JCPDS card no. 34-394). No other secondary phase was detected.

The addition of Sm³⁺ into Ce⁴⁺ can cause a small shift in the ceria peaks. For example, the XRD results indicate that the (2 2 0) peaks of the SDC-PM and SDC-CTM powders shifted downwards by 0.32° and 0.22°, respectively, relative to that of the pure CeO₂ sample at 47.62°. This is because of the larger ionic radius of the samarium ion (0.109 nm) compared to that of the cerium ion (0.097 nm) (Ref 23). This indicates that samarium dissolved into the Ce sites in the Ce_{0.8}Sm_{0.2}O_{1.9} systems prepared by both the Pechini and CT methods. The obtained XRD data are consistent with the literature and include the (111), (200), (220), (311), (222), (400), (331), (420), and (333) diffraction peaks for the two samples.

It can be seen in the XRD results (Fig. 1a) that after calcination at 500 °C, the XRD graph of the SDC-CTM sample presents sharper and narrower peaks than the SDC-PM sample, indicating a greater crystallite size and crystallinity.

The crystallite sizes at 500 °C, as calculated by the Debye-Scherrer equation, were found to be 13 nm for the SDC-CTM powders and 11.2 nm for the SDC-PM powders. Pechini method is a well-proven synthesis technique to obtain powders with small and uniform particle size because this method involves chelating agents and mixing process that enhances the

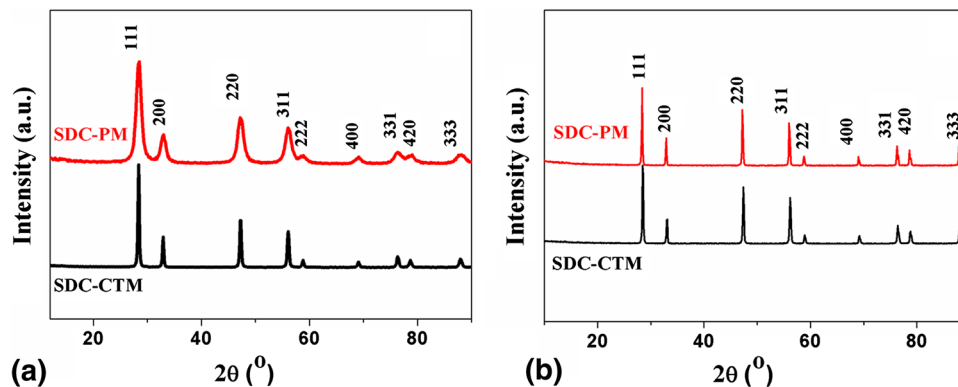


Fig. 1 XRD patterns of (a) SDC-PM and SDC-CTM powders calcined at 500 °C/4 h and (b) SDC-PM and SDC-CTM pellets sintered at 1400 °C/6 h

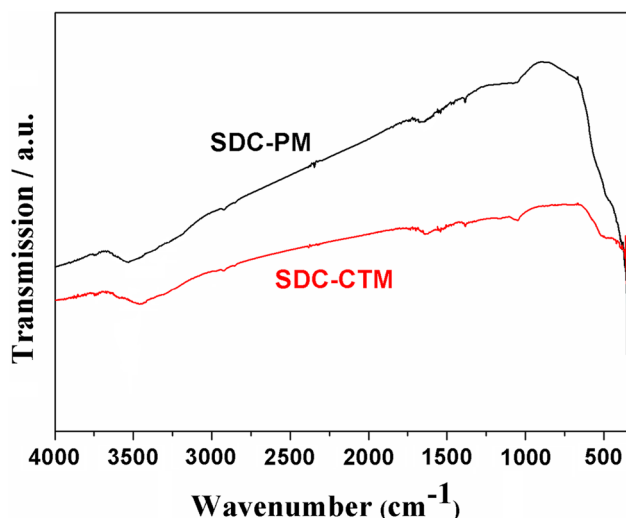


Fig. 2 FTIR spectra of SDC-PM and SDC-CTM powders calcined at 500 °C for 4 h

uniformity of precursors. However in CT method, precursors are impregnated on the cellulose paper and homogeneity depends on the pore size distribution of the microfibrils of the paper. Thus, smaller particles could be obtained with PM compared to CTM. Additionally, more heat might be released during the calcination process of SDC-CTM powders which enhances the crystallinity and therefore the crystallite size of these powders. Nevertheless, the crystallite sizes of the powders are close to each other and these results show the effectiveness of the CT method. As a small crystallite size and good crystallinity are advantageous to obtain dense ceramics in the sintering step, both methods seem to be a good choice for the SOFC electrolyte material synthesis.

As shown in Fig. 1(b), the sintered SDC-PM and SDC-CTM pellets were crystallized into the cubic fluorite structure. The peaks of the sintered samples are sharper than those of the calcined powders, indicating that the sintering process leads to an increased crystallite size and improved crystallinity (Ref 24).

3.2 FTIR Analysis

Figure 2 displays the FTIR transmission spectra of the calcined SDC-PM and SDC-CTM powders. In the spectrum of

the calcined powders, a weak band between 3600 and 3200 cm^{-1} , centered at 3440 cm^{-1} , and a strong intense band below 700 cm^{-1} were observed for the SDC-PM and SDC-CTM powders. The weak peak centered at 3400 cm^{-1} is due to the O-H stretching vibrations attributed to water. After calcination at 500 °C, the band of the O-H stretching vibrations is maintained, probably due to the adsorption of moisture during the testing (The KBr salt used to prepare the pellets for FTIR measurements can easily adsorb water molecules from the air due to hydrogen bond formation on its surface). The FTIR spectra of the calcined SDC-PM and SDC-CTM powders exhibit a strong broad band below 700 cm^{-1} (mostly in the range of 400-650 cm^{-1}) (Ref 25, 26). This band could be attributed to the metal-oxygen bond, which indicates the formation of the samarium-doped ceria (SDC).

3.3 Sintering and Microstructure

Figure 3(a) and (b) show the SEM images of the SDC-PM samples after the calcination process. The powders are foam-like and porous with different sized thin platelets agglomerated. The rapid evolution of the large volume of gases from the combustion of organic materials such as nitrates, citric acid, and ethylene glycol that could not easily escape from the produced powder resulted in localized heating and cooling, which caused nucleation of crystallites without any substantial growth. This phenomenon causes porous or limited interconnected particle networks and the formation of friable agglomerates with different sizes (Ref 27).

The CT method is based on the impregnation of a salt solution into the pores of cellulose filter paper. Figure 3(c) exhibits the SEM images of non-impregnated filter paper. The cellulose paper is compactly packed and has a low void volume. When the metal salt solution was impregnated into the pores of the filter paper and burned out, the mixture of decomposed nitrate salts was entrapped in the free domains of the filter paper. SEM images of the residue that remained after the combustion process are shown in Fig. 3(d). After the removal of the cellulose paper, there is a networked fiber structure of the Sm-Ce-O mixture, consisting of many mesh-like regions.

Sintering directly affects the material properties such as density and grain size. The microstructure of all sintered pellets was examined using SEM. As seen in Fig. 4(a) and (b), the SDC-CTM sample was composed of a dense material, whereas

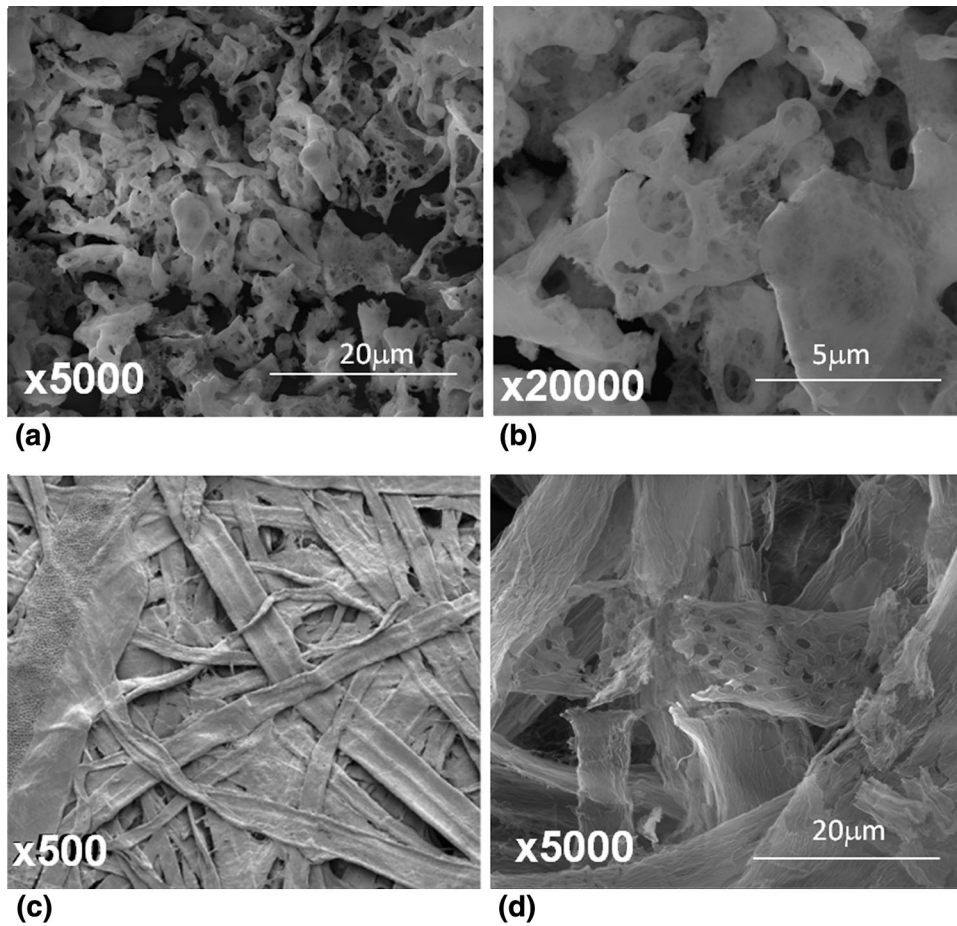


Fig. 3 SEM images of (a and b) SDC-PM powders calcined at 500 °C/4 h and (c) non-impregnated filter paper for CT method. (d) Impregnated and burned-out filter paper at 500 °C/4 h in the CT method

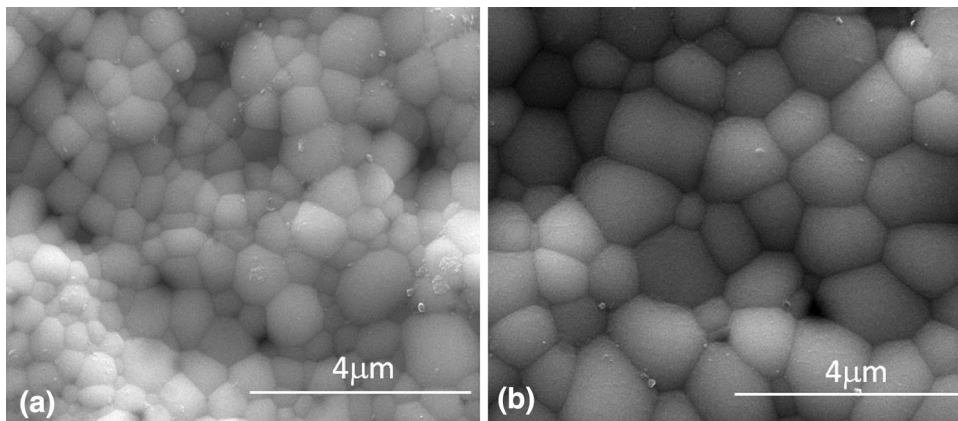


Fig. 4 SEM images of sintered (a) SDC-PM and (b) SDC-CTM pellets at 1400 °C for 6 h ($\times 30,000$)

the SDC-PM sample had few residual pores. Both samples exhibited well-developed straight grain boundaries. The average grain sizes of the sintered samples were measured using SEM images at high magnifications. The average grain size value of the SDC-PM sample was 0.72 μm , while that of the SDC-CTM sample was 1.062 μm . The sintered SDC-CTM pellet had high ionic conductivity because of low resistance of

the grain boundary of the pellet. As seen from the SEM images, the SDC-CTM sample is well sintered, and its relative density value (96%) is higher than that of the SDC-PM sample (91%).

3.4 Ionic Conductivity

Bauerle (Ref 28) introduced for the first time the use of impedance spectroscopy to determine the oxygen ionic

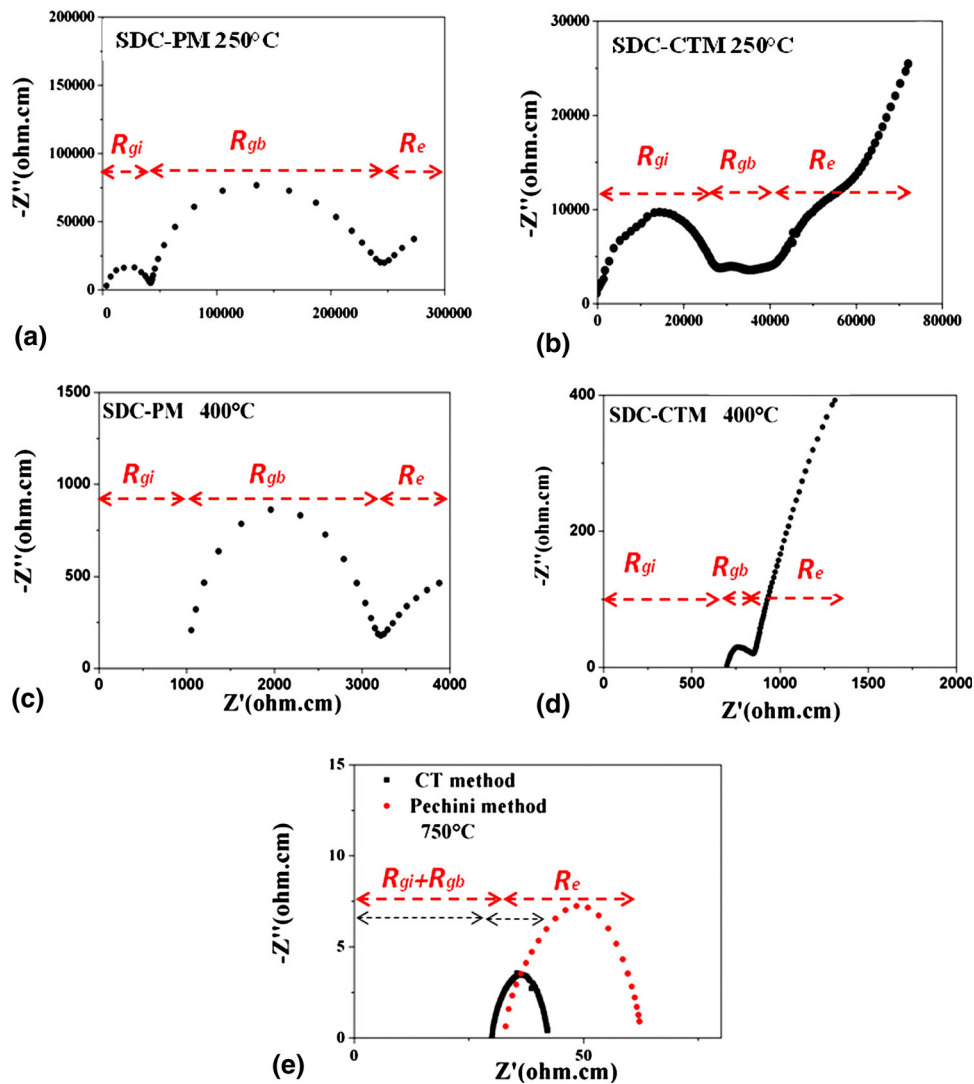


Fig. 5 Complex impedance spectra of (a and c) SDC-PM and (b and d) SDC-CTM pellets sintered at 1400 °C, and measured at 250, 400, and 750°C in air. The grain interior, grain boundary, and electrode contributions are represented as R_{gi} , R_{gb} and R_e , respectively

Table 1 Total conductivity and activation energy of $Ce_{0.8}Sm_{0.2}O_{1.9}$ derived from different fabrication routes

Preparation method	Sintering temp., °C/h	$\sigma_{total} \times 10^2$, S/cm (600 °C)	E , eV	References
Pechini	1400/6	0.86	0.73	This work
Cellulose templating	1400/6	1.74	0.64	This work
Hydrothermal	1450/10	0.20	0.87	Ref 14
Sol-gel	1400/10	0.50	0.97	Ref 16
Ultrasound-microwave assisted sol-gel	1400/2	0.68	...	Ref 17
Carbonate precipitation	1200/4	0.57	0.63	Ref 18

conductivity. SOFC electrolytes are oxygen ion conductors and can therefore be studied using this technique.

Impedance spectroscopy is useful for the study of mobile charges in ionic, semi-conducting, or insulating solids. Moreover, this characterization method can be also used to measure the resistance, or the impedance of the grain boundary, the grain interior (bulk), and the electrode of a sample (Ref 29). The impedance spectra are generally associated with the resistances of grain interior, grain boundary, and electrode, which can be

observed from the first, second, and third arcs. However, all these three arcs can not be observed always together. This case depends on the nature of the samples and conditions of the experiment. The three arcs can be identified clearly at lower temperatures (generally at ≤ 500 °C).

The ionic conductivity measurement was performed in air at a temperature range from 250 to 750 °C. By curve fitting, a circle to the semicircles on the impedance spectra, the sample resistances were obtained as $R_{total} = R_{gi} + R_{gb}$. The conductivity

values were then calculated from the resistances (R), cross-sectional area (A), and thickness (l) using the following equation:

$$\sigma = \frac{l}{AR_{\text{total}}} \quad (\text{Eq 4})$$

The complex impedance spectra plots, which were constructed at temperatures of 250 °C, 400 °C, and 750 °C in air for the sintered SDC-PM and SDC-CTM pellets at 1400 °C, are shown in Fig. 5.

In Fig. 5(a) and (b), two well-defined semicircular arcs, which represent the grain interior (R_{gi}) and grain boundary (R_{gb}), are discernible. As seen from Fig. 5(c) and (d), with increasing operating temperature, the first semicircle on the left side (the high-frequency arc) disappears and only the grain boundary and electrode arcs are observable. When reaching high operating temperatures, the grain interior (R_{gi}) and grain boundary (R_{gb}) resistances become frequency independent, and only one semicircle, which represents the electrode resistance (R_{e}), is visible. At 750 °C, a single arc, which represents the electrode, is observed, as shown in Fig. 5(e).

The grain boundary resistivity of the SDC-PM pellet is higher than that of the SDC-CTM pellet for operating temperatures of 250 and 400 °C. Because the sintered SDC-PM pellet has a smaller grain size (0.72 μm) than the SDC-CTM pellet (1.062 μm), the sintered SDC-PM pellet had a larger percentage of the grain boundary region resulting in the large grain boundary resistivity (Fig. 5a and c). The difference in the grain boundary resistivities of the SDC-PM and SDC-CTM pellets affects the total conductivity. Thus, the observed total conductivity of SDC-CTM is higher than that of SDC-PM. At 750 °C, the grain interior and grain boundary resistances are not discrete, so only the total conductivity can be calculated. At this temperature, the measured total conductivity values of the SDC-PM and SDC-CTM pellets were found to be 3.02×10^{-2} and 3.42×10^{-2} S/cm, respectively.

The ionic conductivity value of doped ceria is affected by different factors such as starting materials, preparation methods, and calcination or sintering temperatures. There are several techniques employed to prepare doped ceria electrolytes (Ref 14, 16-18). In this study, $\text{Sm}_{0.2}\text{Ce}_{0.8}\text{O}_{1.9}$ solid electrolyte material was prepared by using the well-known Pechini and CT methods. The main aim was to study the structure and ionic conductivity of the $\text{Sm}_{0.2}\text{Ce}_{0.8}\text{O}_{1.9}$ electrolyte prepared by the two methods. According to EIS results, the SDC-CTM pellet had a higher total conductivity than the SDC-PM pellet at all measuring temperatures. Nevertheless, the total conductivities of the SDC-PM and SDC-CTM pellets are higher than those of pellets prepared by other preparation methods. The SDC synthesized in this study is compared with materials prepared in the literature in Table 1. When the ionic conductivities of the samples were compared at the same temperature, our samples showed relatively good results. For example, in a study by Huang et al. (Ref 14), they synthesized $\text{Ce}_{0.8}\text{Sm}_{0.2}\text{O}_{1.9}$ using the hydrothermal method and obtained an ionic conductivity value of 0.2×10^{-2} S/cm at 600 °C for a 1450 °C 10 h sintered sample, while we observed 1.74×10^{-2} S/cm at 600 °C for a 1400 °C 6 h sintered SDC-CTM sample. In another study by Huang et al. (Ref 16), they prepared samarium-doped ceria solid electrolytes using the sol-gel method and observed a total conductivity value of 0.5×10^{-2} S/cm at 600 °C. Bu et al. (Ref 17) prepared samarium-doped ceria electrolyte materials by using ultrasound-microwave assisted sol-gel and observed a

conductivity value of 0.68×10^{-2} S/cm at 600 °C. Wang et al. (Ref 18) synthesized $\text{Ce}_{0.8}\text{Sm}_{0.2}\text{O}_{1.9}$ sample via the carbonate precipitation method and obtained an ionic conductivity value of 0.57×10^{-2} S/cm at 600 °C.

The temperature dependence of the ionic conductivities of the electrolytes is illustrated in Fig. 6, and the activation energies were calculated for low and high temperature ranges using the Arrhenius equation. The Arrhenius plots appear linear, but in fact they consist of two lines with different slopes. This difference is because of the change in the conduction mechanism at a specific temperature, which can be taken as the transition temperature (Ref 22, 30). Oxygen ionic conductivity in rare earth-doped ceria can be represented by the following equations:

$$\text{at low temperatures } \sigma = \frac{\sigma_0}{T} e^{-\frac{(\Delta H_m + \Delta H_a)}{kT}}, \quad (\text{Eq 5})$$

$$\text{at high temperatures } \sigma = \frac{\sigma_0}{T} e^{-\frac{\Delta H_m}{kT}}, \quad (\text{Eq 6})$$

where ΔH_m is the migration enthalpy of the oxygen ions and ΔH_a is the association enthalpy of the dopant ion with oxygen vacancies ($k = 8.61 \times 10^{-5}$ eV K^{-1}). Hence, the activation energy (E_a) is the sum of the association enthalpy ΔH_a and migration enthalpy ΔH_m for conduction. At lower temperatures, the activation energy depends on these two contributions. At higher temperatures, the activation energy is equal to the migration enthalpy because oxygen vacancies are free to diffuse (Ref 3, 31).

From Fig. 6 and Table 1, it may be noted that the SDC-CTM pellet showed the highest total ionic conductivity and minimum activation energy. At 600 °C, the ionic conductivity of the SDC-CTM pellet attained a value of 1.74×10^{-2} S/cm,

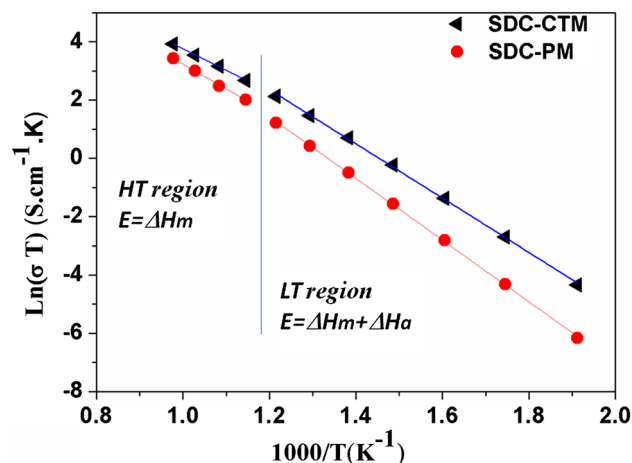


Fig. 6 Arrhenius plots of the SDC-CTM and SDC-PM samples

Table 2 Calculated activation energies of $\text{Ce}_{0.8}\text{Sm}_{0.2}\text{O}_{1.9}$ samples

Samples	E_{total} , eV		$\sigma_{\text{total}} \times 10^{-2}$, S/cm (750 °C)
	LT	HT	
SDC-CTM	0.80	0.64	3.42
SDC-PM	0.91	0.73	3.02

competitive with the previous results measured at the same operating temperature for $\text{Ce}_{0.8}\text{Sm}_{0.2}\text{O}_{1.9}$ ceramics prepared by other synthesis methods (Ref 14, 16-18). The calculated activation energies of $\text{Ce}_{0.8}\text{Sm}_{0.2}\text{O}_{1.9}$ samples produced using two different synthesis methods at 750 °C are provided in Table 2. It seems that the SDC-CTM ceramic is a promising electrolyte material when used in intermediate temperature SOFCs.

4. Conclusions

$\text{Ce}_{0.8}\text{Sm}_{0.2}\text{O}_{1.9}$ powders were successfully synthesized by the Pechini method and CT method. The samarium-doped ceria powders synthesized by both methods have a single-phase fluorite structure at the relatively low calcination temperature of 500 °C. The relative densities of the sintered samples were found to be 96 and 91% for SDC-CTM and SDC-PM, respectively. These findings were consistent with the SEM images.

The synthesis method fairly affected the ionic conductivity properties of the samarium-doped ceria electrolyte at low operating temperatures, but the difference between the ionic conductivities of the SDC pellets prepared by the Pechini and CT methods decreased with increasing operating temperature.

After the sintering process, the grain sizes of the SDC-CTM and SDC-PM pellets were found to be 1.062 and 0.720 μm , respectively. The SDC-CTM pellet had a large grain size and a high conductivity because of the low resistance of the grain boundary of the pellet.

At 750 °C, the SDC-CTM sample exhibited the highest conductivity value of 3.42×10^{-2} S/cm, which is comparable to the literature values. Although the Pechini process is extensively used in the preparation of mixed oxide structures, the CT method is faster and more facile than the Pechini method. Phase purity and relative density are the important factors for obtaining high performance SDC electrolytes. Therefore, the CT method has been demonstrated to be a promising method for the preparation of SDC electrolytes for IT-SOFCs.

Acknowledgments

This work was supported by the Scientific Research Projects Coordination Unit of Istanbul University (Project Numbers 52750, 44373, 42193). It was partially based on a M.Sc. thesis being pursued by Ozgun Serin.

References

- J.P.P. Huijsmans, F.P.F. Van Berkel, and G.M. Christie, Intermediate Temperature SOFC-A Promise for the 21st Century, *J. Power Sources*, 1998, **71**, p 107-110
- H. Yoshida, K. Miura, T. Fukui, S. Ohara, and T. Inagaki, Sintering Behavior of Ln-doped Ceria Compounds Containing Gallia, *J. Power Sources*, 2002, **106**, p 136-141
- B.C.H. Steele, Appraisal of $\text{Ce}_{1-y}\text{Gd}_y\text{O}_{2-y/2}$ Electrolytes for IT-SOFC Operation at 500 °C, *Solid State Ionics*, 2000, **129**, p 95-110
- C. Xia and M. Liu, Microstructures, Conductivities, and Electrochemical Properties of GDC and GDC-Ni Anodes for Low-temperature Solid Oxide Fuel Cells, *Solid State Ionics*, 2002, **152-153**, p 423-430

- J.R. Jurado, Present Several Items on Ceria-Based Ceramic Electrolytes Synthesis, Additive Effects, Reactivity and Electrochemical Behavior, *J. Mater. Sci.*, 2001, **36**, p 1133-1139
- J. VanHerle, T. Horita, T. Kawada, N. Sakai, H. Yokokawa, and M. Dokiya, Low Temperature Fabrication of (Y, Gd, Sm)-Doped Ceria Electrolyte, *Solid State Ionics*, 1996, **86-88**, p 1255-1258
- T. Kudo and H. Obayashi, Oxygen Ion Conduction of the Fluorite-Type $\text{Ce}_{1-x}\text{Ln}_x\text{O}_{2-x/2}$ (Ln = Lanthanoid Element), *J. Electrochem. Soc.*, 1975, **122**(1), p 142-147
- S. Kuharungrong, Ionic Conductivity of Sm, Gd, Dy and Er-Doped Ceria, *J. Power Sources*, 2007, **171**, p 506-510
- T. Karaca, T.G. Altınçekiç, and M.F. Öksüzömer, Synthesis of Nanocrystalline Samarium-Doped CeO_2 (SDC) Powders as a Solid Electrolyte by Using a Simple Solvothermal Route, *Ceram. Int.*, 2010, **36**, p 1101-1107
- M. Chen, B.H. Kim, Q. Xu, B.K. Ahn, W.J. Kang, and D.P. Huang, Synthesis and Electrical Properties of $\text{Ce}_{0.8}\text{Sm}_{0.2}\text{O}_{1.9}$ Ceramics for IT-SOFC Electrolytes by Urea-Combustion Technique, *Ceram. Int.*, 2009, **35**, p 1335-1343
- N. Jaiswal, S. Upadhyay, D. Kumar, and O. Parkash, Ionic Conductivity Investigation in Lanthanum (La) and Strontium (Sr) Co-Doped Ceria System, *J. Power Sources*, 2013, **222**, p 230-236
- E.C.C. Souza and E.N.S. Muccillo, Effect of Solvent on Physical Properties of Samaria-doped Ceria Prepared by Homogeneous Precipitation, *J. Alloys Compd.*, 2009, **473**, p 560-566
- D.Y. Chung and E.H. Lee, Microwave-Induced Combustion Synthesis of $\text{Ce}_{1-x}\text{Sm}_x\text{O}_{2-x/2}$ Powder and Its Characterization, *J. Alloys Compd.*, 2004, **374**, p 69-73
- W. Huang, P. Shuk, and M. Greenblatt, Hydrothermal Synthesis and Properties of $\text{Ce}_{1-x}\text{Sm}_x\text{O}_{2-x/2}$ and $\text{Ce}_{1-x}\text{Ca}_x\text{O}_{2-x}$ Solid Solutions, *Chem. Mater.*, 1997, **9**(10), p 2240-2245
- D.J. Seo, K.O. Ryu, S.B. Park, K.Y. Kim, and R.H. Song, Synthesis and Properties of $\text{Ce}_{1-x}\text{Gd}_x\text{O}_{2-x/2}$ Solid Solution Prepared by Flame Spray Pyrolysis, *Mater. Res. Bull.*, 2006, **41**, p 359-366
- W. Huang, P. Shuk, and M. Greenblatt, Properties of Sol-Gel Prepared $\text{Ce}_{1-x}\text{Sm}_x\text{O}_{2-x/2}$ Solid Electrolytes, *Solid State Ionics*, 1997, **100**, p 23-27
- Y. Bu, Q. Zhong, W. Tan, R. Zhou, Y. Song, and W. Cai, Synthesis and Properties of Samaria-Doped Ceria Electrolyte Via Ultrasound-Microwave Assisted Sol-Gel Method, *Mater. Sci. Semicond. Proc.*, 2013, **16**, p 2058-2062
- Y. Wang, T. Mori, J.G. Li, and Y. Yajima, Low-Temperature Fabrication and Electrical Property of 10 mol% Sm_2O_3 -Doped CeO_2 Ceramics, *Sci. Technol. Adv. Mater.*, 2003, **4**(3), p 229-238
- H. Özdemir, V. Sariboga, M.A.F. Öksüzömer, and M.A. Gürkaynak, Preparation and Characterization of Ca-Sm-Ce Mixed Oxides via Cellulose Templating Method for Solid Oxide Fuel Cell Applications, *J. Power Sources*, 2012, **219**, p 155-162
- K. Langfeld, R. Marschner, B. Frank, and R. Schomaker, Methane Activation over Cellulose Templated Perovskite Catalysts, *ChemCatChem*, 2011, **3**(8), p 1354-1358
- B. Uslu, A. Aytimur, M.K. Ozturk, and S. Kocyigit, Synthesis and Characterization of Neodymium Doped Ceria Nanocrystalline Ceramic Structures, *Ceram. Int.*, 2012, **38**(6), p 4943-4951
- S. Zha, C. Xia, and G. Meng, Effect of Gd(Sm) Doping on Properties of Ceria Electrolyte for Solid Oxide Fuel Cells, *J. Power Sources*, 2003, **115**, p 44-48
- J. Kimpton, T.H. Randle, and J. Drennan, Investigation of Electrical Conductivity as a Function of Dopant-Ion Radius in the Systems $\text{Zr}_{0.75}\text{Ce}_{0.08}\text{M}_{0.17}\text{O}_{1.92}$ (M = Nd, Sm, Gd, Dy, Ho, Y, Er, Yb, Sc), *Solid State Ionics*, 2002, **149**(1-2), p 89-98
- S. Panigrahi, R.C. Biswal, S. Anwar, L. Besra, and S. Bhattacharjee, Temperature Dependence of Ionic Conductivity of Ceria Electrolyte at Concentrated Range of Multiple Doping, *J. Am. Ceram. Soc.*, 2013, **96**(9), p 2846-2851
- S. Kundu, N. Sutradhar, R. Thangamuthu, B. Subramanian, A.B. Panda, and M. Jayachandran, Fabrication of Catalytically Active Nanocrystalline Samarium (Sm)-doped Cerium Oxide (CeO_2) Thin Films Using Electron Beam Evaporation, *J. Nanopart. Res.*, 2012, **14**, p 1040-1056
- K.C. Anjaneya, G.P. Nayaka, J. Manjanna, G. Govindaraj, and K.N. Ganesha, Preparation and Characterization of $\text{Ce}_{1-x}\text{Sm}_x\text{O}_{2-d}$ ($x = 0.1-0.3$) as Electrolyte Material for Intermediate Temperature SOFC, *Solid State Sci.*, 2013, **26**, p 89-96

27. R.V. Mangalaraja, S. Ananthakumar, A. Schachtsiek, M. López, C.P. Camurri, and R.E. Avilad, Synthesis and Mechanical Properties of Low Temperature Sintered, Sm^{3+} Doped Nanoceria Electrolyte Membranes for IT-SOFC Applications, *Mater. Sci. Eng., A*, 2010, **527**, p 3645–3650
28. J.E. Bauerle, Study of Solid Electrolyte Polarization by a Complex Admittance Method, *J. Phys. Chem. Solids*, 1969, **30**(12), p 2657–2670
29. J. Luo, R.J. Ball, and R. Stevens, Gadolinia Doped Ceria/Yttria Stabilised Zirconia Electrolytes for Solid Oxide Fuel Cell Applications, *J. Mater. Sci.*, 2004, **39**, p 235–240
30. S. Omar, E.D. Wachsman, and J.C. Nino, Higher Conductivity Sm^{3+} and Nd^{3+} Co-Doped Ceria-Based Electrolyte Materials, *Solid State Ionics*, 2008, **178**, p 1890–1897
31. H. Inaba and H. Tagawa, Ceria-Based Solid Electrolyte, *Solid State Ionics*, 1996, **83**(1–2), p 1–16